Meter-Scale Terahertz-Driven Acceleration of a Relativistic Beam

E. Curry,[1,*] S. Fabbri,[1] J. Maxson,[1,†] P. Musumeci,[1] and A. Gover[2]
[1]*Department of Physics and Astronomy, UCLA, Los Angeles, California 90095, USA*
[2]*Faculty of Engineering, Department of Physical Electronics, Tel-Aviv University, Tel-Aviv 69978, Israel*

(Received 27 October 2017; published 28 February 2018)

Terahertz (THz) radiation promises breakthrough advances in compact advanced accelerators due to the gigavolts-per-meter fields achievable, but the challenge of maintaining overlap and synchronism between beams and short laser-generated THz pulses has so far limited interactions to the few-millimeter scale. We implement a novel scheme for simultaneous group and phase velocity matching of nearly single-cycle THz radiation with a relativistic electron beam for meter-scale inverse free-electron laser interaction in a magnetic undulator, resulting in energy modulations of up to 150 keV using modest THz pulse energies (≤ 1 μJ). Using this scheme, we demonstrate for the first time the use of a laser-based THz source for bunch-length compression and time-stamping of a relativistic electron beam.

DOI: 10.1103/PhysRevLett.120.094801

The continuous progress in the development of high peak and average power sources in the terahertz (THz) frequency range is closely followed by modern accelerator and beam physics, as THz waves bridge the gap between radio frequencies and laser frequencies in accelerator applications. THz-based acceleration combines key advantages from both regimes, sustaining high-gradient fields while retaining a broad temporal acceptance window. Important proof-of-principle results have recently been obtained using corrugated waveguides and dielectric-based structures. For example, using an iris-loaded waveguide structure, an acceleration of 7 keV in 6 mm was reported by Nanni *et al.* [1]. Similarly, THz waves have been successfully used to accelerate and manipulate electron beams at the injector [2–4] and in nonrelativistic beam lines [5,6].

Beam-based THz sources have demonstrated very high power and efficiency [7]. O'Shea *et al.* observed an energy gradient over 1 GeV/m using a beam-driven dielectric wakefield accelerator in the THz regime [8]. However, these sources are dependent upon the availability of high-energy, high-current drive electron beams [9,10]. Laser-based THz sources [11,12] utilize ultrafast laser systems and access very high (up to gigavolts per meter) electric fields even with modest pulse energy due to the short pulse width (near single-cycle) of the generated radiation. The compactness, flexible temporal structure and inherent synchronization with an external laser signal make a laser-based THz source uniquely attractive for beam manipulation and diagnosis. Optical rectification in nonlinear crystals is particularly appealing, given the prospects for improving conversion efficiency and scaling to higher THz pulse energies [13–16] and harnessing peak field enhancement [17,18].

The short duration of near-single-cycle pulses from laser-based THz sources strongly limits the temporal overlap between the electron beam and the high-intensity THz field [19–21]. In metallic or dielectric structures, it is difficult to simultaneously tune both the phase and the group velocity of the radiation, as required to keep the particles overlapped with the THz pulse envelope, while riding at a constant accelerating or decelerating phase [22,23]. The resulting group velocity mismatch quickly degrades the efficiency of the energy exchange, posing a severe limitation on the length of the interaction (typically $\leq$ a few millimeters).

In Ref. [24], we presented a THz-driven inverse free-electron laser (IFEL) scheme in which the duration of interaction can be dramatically increased using a curved parallel plate waveguide (CPPWG) to match both the THz group and the phase velocity for resonant interaction. This "zero-slippage" IFEL scheme allows coupling to a broad spectral bandwidth and large transverse acceptance, only limited by the waveguide aperture. Furthermore, the waveguide counteracts the transverse spread of the THz pulse due to diffraction, extending the length along which efficient energy exchange occurs to a meter-scale interaction.

In this Letter, we discuss the first experimental demonstration of this scheme (see Fig. 1). By copropagating a broad-bandwidth 1 μJ THz pulse with a 4–9 MeV high-brightness electron beam from an rf photoinjector [25] in a 30-cm-long planar undulator and CPPWG, we observed up to 150 keV peak-to-peak induced energy modulation. Results from beam energy scans at different CPPWG spacings are used to demonstrate the resonant nature of the interaction and validate our model and understanding of this scheme [26]. The energy modulation was observed to scale linearly with the THz field amplitude as expected, opening the door to scaling this scheme to significantly higher energies. Longitudinal phase space (LPS) measurements of a multi-picosecond-input electron beam reveal the

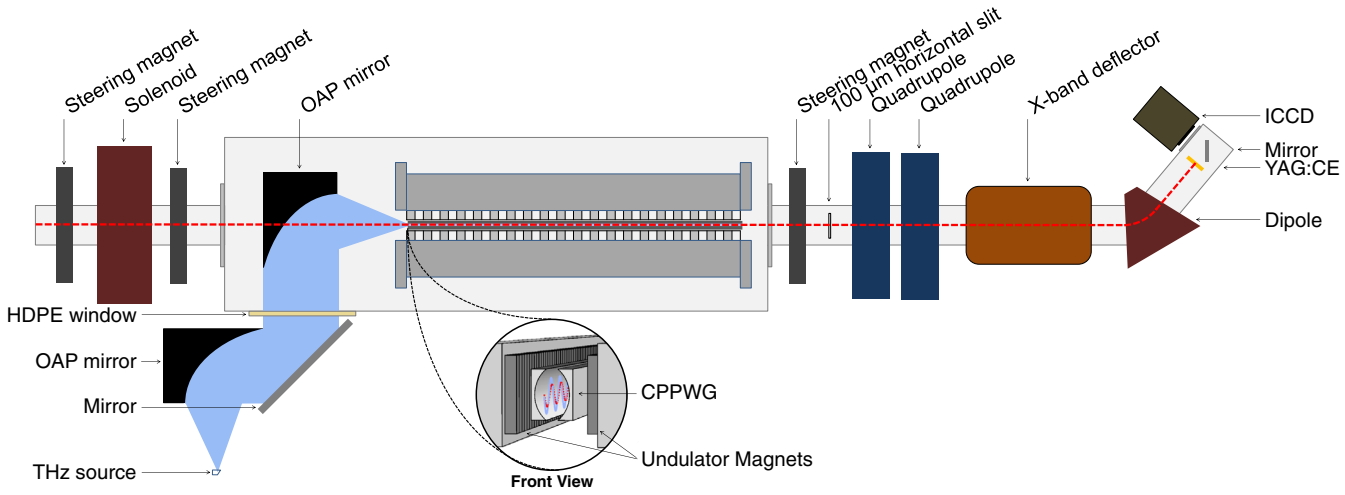

FIG. 1. Diagram of the experimental area on the PEGASUS beam line (not to scale), with inset view of the undulator entrance and curved parallel plate waveguide (CPPWG), showing the electron beam (dashed red) and THz (light blue) path. THz radiation, generated via pulse-front-tilted optical rectification of 1 mJ of an 800 nm laser in stoichiometric lithium niobate (sLN), was transported to the CPPWG using a system of off-axis parabolic (OAP) mirrors. A camera located outside the vacuum chamber imaged the CPPWG aperture, controlled via a tunable six-axis self-centering mount, to determine the spacing with 100 μm accuracy. A solenoid focused the beam through a 2 mm hole in the THz-focusing OAP mirrors to a 200 μm waist at the entrance of the planar Halbach-style undulator. Downstream, a dipole magnet horizontally disperses the energy distribution onto a fluorescent high-yield spectrometer screen. A 9.6 GHz transverse deflecting cavity could be used to streak the longitudinal beam profile onto the vertical axis.

full sinusoidal energy modulation due to the THz field and can be used to retrieve the relative time of arrival between electrons and radiation. Shortening the electron beam to subcycle bunch length, an initial demonstration of THz-driven bunch-length compression was also carried out, resulting in a factor-of-2 temporal compression.

The IFEL interaction in a planar undulator is governed by the phase synchronism condition, given in terms of the THz frequency ω as

$$\frac{\omega}{c\bar{\beta}_z} = k_z(\omega) + k_u \tag{1}$$

for a given undulator of period $2\pi/k_u$ and normalized magnetic field amplitude $K = (eB_u/k_u mc)$. In typical plane-wave free-space interaction, IFEL phase matching is possible only for one frequency [see Fig. 2(a)], and thus no group velocity matching; with the waveguide, the THz and electron beam dispersion curves can be tangent to each other, indicating group velocity matching and broadband interaction. Phase synchronism can be satisfied by adjusting either the normalized longitudinal electron velocity $\bar{\beta}_z = \sqrt{1-(1+K^2/2/\gamma^2)}$ or the THz wave number $k_z(\omega)$, whose ω dependence is set by the CPPWG plate spacing. The extra degree of freedom can be used to match the THz group velocity with the electron propagation $\bar{\beta}_z$, resulting in a "zero-slippage" interaction, wherein the electron bunch and THz pulse remain overlapped throughout the undulator [24]. This matching is indicated by the intersection in Fig. 2(b). Increasing the waveguide spacing results in a smaller resonant beam energy, because while the THz group velocity increases, the phase velocity decreases. Dispersion and diffraction of the THz pulse in the waveguide, as well as coupling efficiency, affect the strength of the interaction for different waveguide spacings [24].

The undulator field was tuned via adjustments to the magnet gap (14 mm) based on Hall probe measurements and a Radia 3D simulation model [27]. The optimal THz pulse timing was determined by adjusting a THz source delay stage while measuring the induced energy spread; see Fig. 3(a). The temporal duration of the interaction is a convolution of

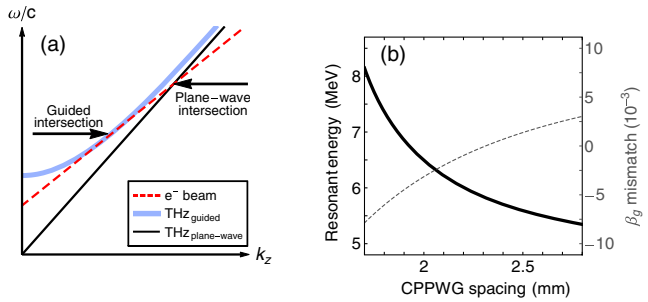

FIG. 2. (a) IFEL phase synchronism is given by the intersection between dispersion curves for the electrons oscillating in the undulator (dashed red) and the THz radiation, for free-space plane-wave propagation (black) and waveguide propagation (light blue). Tangential intersection indicates group velocity matching (not to scale). (b) Resonant beam energy as determined by CPPWG spacing using the parameters given in Table I at a single THz frequency (black). The corresponding group velocity mismatch is shown (dashed gray line with scale indicated on right axis).

TABLE I. IFEL experimental parameters.

Bunch energy	4–9 MeV
Undulator period	3 cm
Undulator parameter, K	1.27
Number of undulator periods	10
CPPWG spacing, b	1.5–3 mm
Plate curvature radius	2 mm
Peak frequency	0.84 THz
Pulse energy	1 μJ

the electron bunch and THz pulse lengths. Consecutive beam images display the electron energy spectrum for THz on [Fig. 3(b)] and off [Fig. 3(c)] from the peak of this timing scan. The induced energy spread is quantified by the full width full max (FWFM) of a small vertical slice in the image, defined here as the width of the energy distribution at 10% of the peak value. The initial beam energy was tuned and the energy spread was minimized (30 keV FWFM) by adjusting the amplitude and phase of the 1.6 cell S-band gun and booster linac.

Measurements were first taken using an electron beam with approximately 1.5 ps rms bunch length, covering multiple periods of the THz waveform to increase the temporal overlap window. As a result, electrons were injected over all interaction phases, with some accelerated and some decelerated; the modulated energy distribution was symmetrically widened with respect to the initial distribution [see bottom of Figs. 3(b) and 3(c)]. The full width of the final spectrum can be as large as 150 keV, in good agreement with our simulation model. The maximum energy gain (or loss) for single particles is estimated at one half of the deconvolution of the initial and final distribution. Note that dispersion in the CPPWG stretches the broadband THz pulse to a few-cycle pulse, with a varying field amplitude determined by the overall pulse envelope. The discontinuous steps visible in the projected energy distribution of the THz "on" shot are the result of the multicycle nature of the energy modulation, with portions of the beam undergoing different modulation amplitudes. This feature is evident in simulations and LPS measurements of the beam distribution [see Fig. 4(a)].

To demonstrate waveguide-based tuning of the IFEL phase-matching condition, we performed measurements over a range of beam energies for different waveguide spacings [1.8 mm and 2.4 mm are shown in Fig. 3(d)]. Each point represents the maximum energy spread at a particular beam energy. For smaller plate spacing, the resonant energy increases, consistent with our simple model of the interaction.

A simulation code which takes into account the different coupling efficiency as well as dispersion in the CPPWG was developed to understand quantitatively the strength of the beam-radiation interaction. Coupling efficiency of the THz pulse into the waveguide is calculated using the transverse profile overlap integral of free-space and waveguide modes. The code then tracks particles through both the undulator field and the THz field, which evolves in the frequency domain from an initial waveform which was independently determined via electro-optic sampling (EOS) measurements. The initial beam energy spread is given by spectrometer images with the THz source off. Total charge was kept below 1 pC to minimize feedback of the electron beam bunching on the radiation evolution. The simulation results reported in Fig. 3(d) assume 25% power coupling of the 1 μJ THz pulse, measured at the sLN crystal, yielding an estimate of 4–8 MV/m for the maximum THz field of the TE_{01} mode. Residual differences in FWFM are ascribed to experimental uncertainties related to the coupling of the THz pulse into the guide, misalignment of the CPPWG plates, and alignment of the electron beam through the guide and undulator axis. Note that additional interaction with higher-order modes in the waveguide might further contribute to particle acceleration or deceleration,

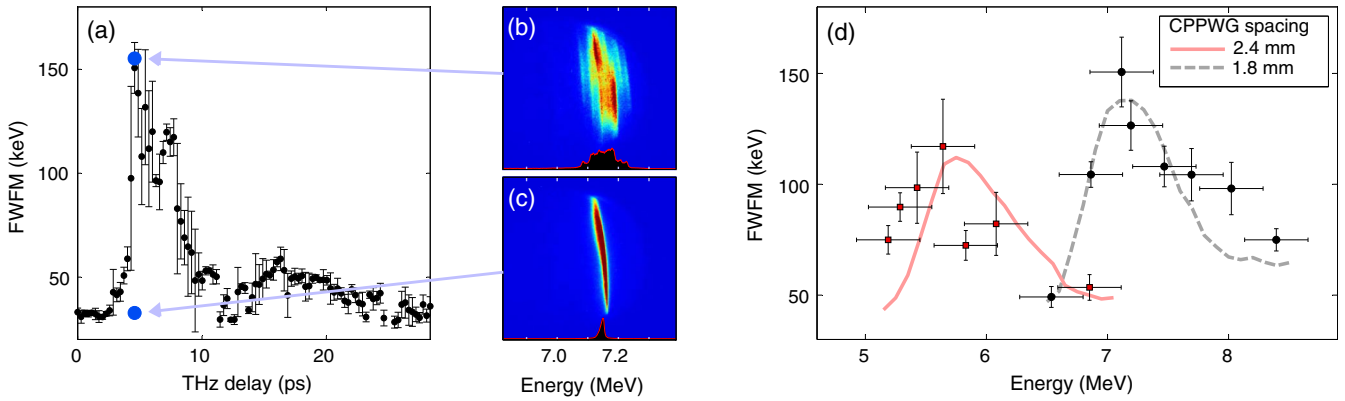

FIG. 3. (a) Plot of beam energy spread vs THz arrival time with example beam images for THz (b) on and (c) off indicated by blue arrows. The energy distribution is projected at the bottom of each beam image. (d) Scan of the maximum induced energy spread vs beam energy for two plate spacings. Each point is an average of "on" shots from the delay corresponding to peak energy modulation. Lines indicate the FWFM energy modulation from simulation.

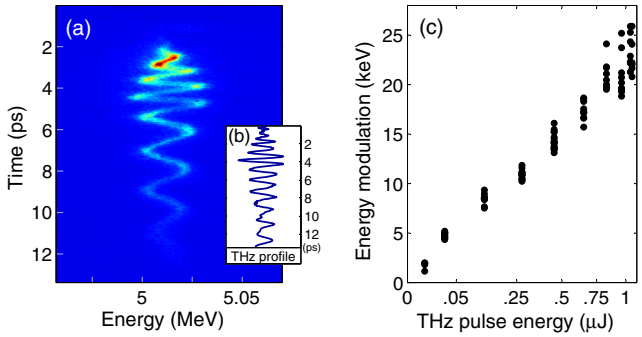

FIG. 4. (a) Longitudinal phase-space measurement, with beam image transformed to remove residual rf curvature. (b) Inset showing the predicted THz pulse profile after a 30 cm CPPWG, based on EOS measurements of the initial pulse. (c) Maximum peak-to-peak energy modulation taken from LPS images for a range of measured THz energies, using 5 MeV beam energy and 2.7 mm waveguide spacing. A quadratic x-axis scale shows the linear relationship between the THz field and energy modulation.

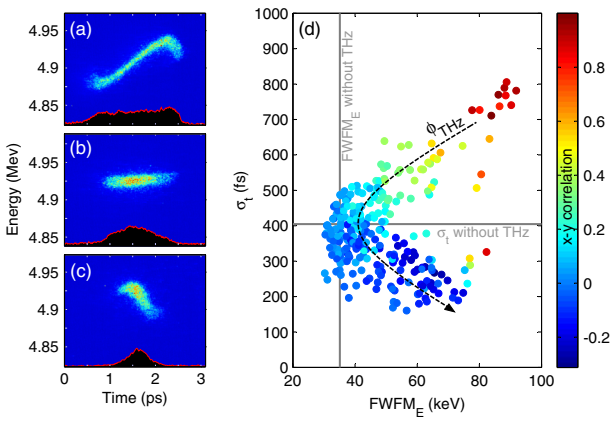

FIG. 5. LPS images showing the short beam (a) with positive energy chirp, resulting in decompression; (b) unmodulated with THz off; and (c) with negative energy chirp, resulting in compression. The temporal distribution is projected at the bottom of each beam image. (d) Plot of rms bunch length vs energy spread, with color determined by energy-position correlation, for many LPS images. As expected, positive (warm) and negative (cool) correlation correspond to decompression and compression of the beam, respectively. Gray lines show the mean energy spread and bunch length of the beam without THz interaction. An arrow highlights the transition in the THz interaction phase from decompression to compression.

though this effect is calculated to be responsible for less than 10% of the induced energy spread.

A more complete picture of the interaction is gained from images of the beam LPS, wherein we map the energy gain vs bunch temporal coordinate [see Fig. 4(a)]. After the IFEL, the beam was deflected vertically in an X-band cavity before undergoing the energy-dependent deflection in the dipole magnet [28]. A slit was used to limit the Panfosky-Wenzel deflector-induced energy spread to <10 keV, and two quadrupoles minimized the betatron beam sizes on the screen [29]. The LPS measurements reveal the multicycle energy modulation that we expected from interaction with the dispersed THz pulse [see Fig. 4(b)].

A direct measurement of the beam time-of-arrival jitter with respect to the THz pulse can be obtained by monitoring the position of the energy modulation with respect to the beam head and yields 400 fs rms temporal jitter, in agreement with previous measurements on the PEGASUS beam line [30]. The maximum peak-to-peak energy modulation can be directly measured after filtering to remove background and subtracting off the underlying rf curvature-induced energy chirp. Varying the THz energy, controlled by laser power illuminating the sLN crystal, yields the expected linear relation between the maximum energy modulation and the THz field amplitude [see Fig. 4(c)]. Note that the data here correspond to a larger than optimal waveguide spacing and low incident THz field, so that the interaction was not maximized.

One attractive application of this interaction is bunch-length compression: a negative energy chirp induced in a short beam injected at a zero crossing of the wave with a subsequent dispersive section to allow faster particles in the tail to catch up with the head. The high frequency of the THz wave results in a steep energy chirp with only modest field amplitude. Additionally, the LPS rotation of the beam relative to the inherent, ideal timing synchronization of the laser-generated THz pulse can reduce the overall beam timing jitter [24].

After recompressing the photocathode driver laser (100 fs pulse length) to produce a beam short enough to fit in the linear part of the THz wave, we tested this concept for THz-driven bunch compression. Because of the large beam timing jitter associated with amplitude and phase fluctuations in the aging rf system at PEGASUS, consecutive shots sampled a wide range of injection phases in the THz waveform, resulting in a corresponding range of induced energy chirps. Depending on the sign of the energy-position correlation, the subsequent drift decompressed or compressed the beam, as shown in Fig. 5(d) with warm and cool colors indicating positive and negative correlations, respectively.

When the beam is injected at a THz phase with positive field gradient (so that the head is accelerated to higher energy than the tail), the energy spread increases, and the final bunch LPS is elongated with a positive energy-position correlation, as in Fig. 5(a). If the beam interaction phase corresponds to little overall field gradient, there is minimal energy chirp—i.e., near-zero energy-position correlation—and the energy spread and bunch length are largely unchanged.

Ideally, the dispersion following the undulator is sufficient to allow the back of the bunch to catch the head upon reaching the rf streak camera. For the LPS measurements discussed here, the available 1 m drift was too short to obtain

full compression. Even at the shortest bunch lengths, beam images still show a nonzero energy-position correlation, as in Fig. 5(c). However, as shown in Fig. 5(d), the bunch length did decrease to a minimum of 200 fs, demonstrating THz-driven bunch compression. Peripheral LPS aberrations, easily noticeable in Figs. 5(a) and 5(c), resulted from the initial bunch length (400 fs rms) being too large to fit fully within a half period of the THz waveform.

The results of the zero-slippage IFEL coupling scheme presented here show a flexible technique for THz-driven beam manipulation which can be employed to energy-modulate, time-stamp, or temporally compress a relativistic electron beam. The group and phase velocity matched interaction allowed sustained coupling for up to 30 cm, a drastic increase over the few millimeters previously demonstrated in other THz-based acceleration schemes, and enabled a record high-energy modulation of 150 keV using a 1 μJ energy THz pulse with < 10 MV/m peak field. As we demonstrated, energy gain and gradient scale linearly with the initial THz field. Therefore, the small acceleration gradient achieved, 0.25 MeV/m, could be increased by more than 2 orders of magnitude using state-of-the-art THz sources. Generation techniques are improving rapidly, and millijoule-class THz pulses with peak fields approaching gigavolts per meter are already available [1,2]. Moreover, due to the group-velocity-matching properties of the zero-slippage scheme, the energy modulation could be further increased by extending the undulator and CPPWG length, only limited by dispersive pulse broadening and attenuation losses.

Further applications of the coupling scheme include transverse deflection for longitudinal beam diagnostics [26] (using an odd-symmetry mode in the waveguide), and ultimately THz broadband amplification when a high-charge beam is decelerated in a tapered undulator [31].

This work has been supported by DOE Grant No. DE-SC0009914 and NSF Grants No. PHY-1415583 and No. PHY-1734215, with partial support by the US-Israel Binational Science Foundation (BSF). The authors acknowledge useful discussions with G. Andonian and D. Cesar.

*ejcurry@physics.ucla.edu
†Present address: CLASSE, Cornell University, 161 Synchrotron Drive, Ithaca, New York 14853-8001, USA.

[1] E. A. Nanni, W. R. Huang, K. Ravi, A. Fallahi, G. Moriena, R. J. Miller, and F. X. Kärtner, Terahertz-driven linear electron acceleration, Nat. Commun. **6**, 8486 (2015).
[2] W. R. Huang, A. Fallahi, X. Wu, H. Cankaya, A.-L. Calendron, K. Ravi, D. Zhang, E. A. Nanni, K.-H. Hong, and F. X. Kärtner, Terahertz-driven, all-optical electron gun, Optica **3**, 1209 (2016).
[3] A. Fallahi, M. Fakhari, A. Yahaghi, M. Arrieta, and F. X. Kärtner, Short electron bunch generation using single-cycle ultrafast electron guns, Phys. Rev. ST Accel. Beams, **19**, 081302 (2016).
[4] L. Wimmer, G. Herink, D. R. Solli, S. V. Yalunin, K. E. Echternkamp, and C. Ropers, Terahertz control of nanotip photoemission, Nat. Phys. **10**, 432 (2014).
[5] C. Kealhofer, W. Schneider, D. Ehberger, A. Ryabov, F. Krausz, and P. Baum, All-optical control and metrology of electron pulses, Science **352**, 429 (2016).
[6] U. Frühling, M. Wieland, M. Gensch, T. Gebert, B. Schütte, M. Krikunova, R. Kalms, F. Budzyn, O. Grimm, J. Rossbach *et al.*, Single-shot terahertz-field-driven x-ray streak camera, Nat. Photonics **3**, 523 (2009).
[7] Z. Wu, A. S. Fisher, M. C. Hoffmann, S. Bonetti, D. Higley, and H. Durr, Terahertz light source at SLAC FACET user facility, in *39th International Conference on Infrared, Millimeter, and Terahertz Waves (IRMMW-THz)* (IEEE, New York, 2014), pp. 1–2.
[8] B. D. O'Shea, G. Andonian, S. K. Barber, K. L. Fitzmorris, S. Hakimi, J. Harrison, P. D. Hoang, M. J. Hogan, B. Naranjo, O. B. Williams, V. Yakimenko, and J. B. Rosenzweig, Observation of acceleration and deceleration in gigaelectron-volt-per-metre gradient dielectric wakefield accelerators, Nat. Commun. **7**, 12763 (2016).
[9] S. Antipov, M. Babzien, C. Jing, M. Fedurin, W. Gai, A. Kanareykin, K. Kusche, V. Yakimenko, and A. Zholents, Subpicosecond Bunch Train Production for a Tunable Millijoule Level Terahertz Source, Phys. Rev. Lett. **111**, 134802 (2013).
[10] F. Giorgianni *et al.*, Strong nonlinear terahertz response induced by Dirac surface states in Bi_2Se_3 topological insulator, Nat. Commun. **7**, 11421 (2016).
[11] K.-L. Yeh, M. C. Hoffmann, J. Hebling, and K. A. Nelson, Generation of 10 μJ ultrashort terahertz pulses by optical rectification, Appl. Phys. Lett. **90**, 171121 (2007).
[12] J. Hebling, K.-L. Yeh, M. C. Hoffmann, and K. A. Nelson, High-power terahertz generation, terahertz nonlinear optics, and terahertz nonlinear spectroscopy, IEEE J. Sel. Top. Quantum Electron. **14**, 345 (2008).
[13] J. A. Fülöp, L. Pálfalvi, M. C. Hoffmann, and J. Hebling, Towards generation of millijoule-level ultrashort terahertz pulses by optical rectification, Opt. Express **19**, 15090 (2011).
[14] S.-W. Huang, E. Granados, W. R. Huang, K.-H. Hong, L. E. Zapata, and F. X. Kärtner, High conversion efficiency, high energy terahertz pulses by optical rectification in cryogenically cooled lithium niobate, Opt. Lett. **38**, 796 (2013).
[15] C. Vicario, B. Monoszlai, and C. P. Hauri, Gigavolts-per-Meter Single-Cycle Terahertz Fields from a Laser-Driven Large-Size Partitioned Organic Crystal, Phys. Rev. Lett. **112**, 213901 (2014).
[16] S. W. Jolly, F. Ahr, N. H. Matlis, S. Carbajo, K. Ravi, T. Kroh, J. Schulte, D. N. Schimpf, A. R. Maier, and F. X. Kärtner, Narrowband terahertz generation with broadband chirped pulse trains in periodically poled lithium niobate, in *CLEO: QELS_Fundamental Science*, (Optical Society of America, 2015), paper FW4D-4.
[17] S. Bagiante, F. Enderli, J. Fabiańska, H. Sigg, and T. Feurer, Giant electric field enhancement in split ring resonators featuring nanometer-sized gaps, Sci. Rep. **5**, 8051 (2015).
[18] J. Fabiańska, G. Kassier, and T. Feurer, Split ring resonator based terahertz-driven electron streak camera featuring femtosecond resolution, Sci. Rep. **4**, 5645 (2014).

[19] J. T. Moody, R. K. Li, P. Musumeci, C. M. Scoby, and H. To, Compression and synchronization of an ultra-short electron beam using a THz undulator interaction, in *Conference Proceedings* (2011), Vol. 110328, No. PAC-2011-WEP189, pp. 1843–1845.

[20] S. P. Jamison, M. J. Cliffe, D. M. Graham, T. Thakker, B. Muratori, Y. M. Saveliev, and R. J. Smith *et al.*, Phase space manipulation with laser-generated terahertz pulses, in *34th International Free Electron Laser Conference* (2012).

[21] J. Hebling, J. A. Fülöp, M. I. Mechler, L. Pálfalvi, C. Tőke, and G. Almási, Optical manipulation of relativistic electron beams using terahertz pulses, arXiv:1109.6852.

[22] L. J. Wong, A. Fallahi, and F. X. Kärtner, Compact electron acceleration and bunch compression in terahertz waveguides, Opt. Express **21**, 9792 (2013).

[23] D. A. Walsh, D. S. Lake, E. W. Snedden, M. J. Cliffe, D. M. Graham, and S. P. Jamison, Demonstration of sub-luminal propagation of single-cycle terahertz pulses for particle acceleration, Nat. Commun. **8**, 421 (2017).

[24] E. Curry, S. Fabbri, P. Musumeci, and A. Gover, Terahertz-driven zero-slippage IFEL scheme for phase space manipulation, New J. Phys. **18**, 113045 (2016).

[25] D. Alesini, A. Battisti, M. Ferrario, L. Foggetta, V. Lollo, L. Ficcadenti, V. Pettinacci, S. Custodio, E. Pirez, P. Musumeci, and L. Palumbo, New technology based on clamping for high gradient radio frequency photogun, Phys. Rev. ST Accel. Beams **18**, 092001 (2015).

[26] E. Curry, S. Fabbri, P. Musumeci, and A. Gover, Simulation of 3D effects in terahertz-based phase space manipulation, Nucl. Instrum. Methods Phys. Res., Sect. A **865**, 67 (2017).

[27] O. Chubar, P. Elleaume, and J. Chavanne, A three-dimensional magnetostatics computer code for insertion devices, J. Synchrotron Radiat. **5**, 481 (1998).

[28] J. Maxson, D. Cesar, G. Calmasini, A. Ody, P. Musumeci, and D. Alesini, Direct Measurement of Sub-10-fs Relativistic Electron Beams with Ultralow Emittance, Phys. Rev. Lett. **118**, 154802 (2017).

[29] J. T. Moody, P. Musumeci, M. S. Gutierrez, J. B. Rosenzweig, and C. M. Scoby, Longitudinal phase space characterization of the blow-out regime of rf photoinjector operation, Phys. Rev. ST Accel. Beams **12**, 070704 (2009).

[30] D. B. Cesar, P. Musumeci, and D. Alesini, Ultrafast gating of a mid-infrared laser pulse by a sub-picocoulomb relativistic electron beam, J. Appl. Phys. **118**, 234506 (2015).

[31] J. P. Duris, A. Murokh, and P. Musumeci, Tapering enhanced stimulated super-radiant amplification, New J. Phys. **17**, 063036 (2015).